AIAA JOURNAL
Vol. 40, No. 2, February 2002

Aperture Effects on the Aerooptical Distortions Produced by a Compressible Shear Layer

Edward J. Fitzgerald* and Eric J. Jumper†
University of Notre Dame, Notre Dame, Indiana 46556

A recent paper presented time-series measurements of optical wave front distortions produced by a weakly compressible shear layer using the small-aperture beam technique (SABT). These researchers used a posttest, high-pass, digital filter to remove vibrational noise from their beam-jitter signals, choosing a corner-frequency compatible with their 5-cm test aperture. A reexamination of their raw data is documented, and the proper corner-frequency selection for vibration-corruption removal is systematically treated. The resulting SABT wave front reconstructions recaptured the structures previously reported, but now reveal large-amplitude, time-varying, tilt aberrations not previously of interest to 5-cm-aperture optical-system applications. These tilt aberrations are indicative of large-scale flow structures with a spatial scale larger than the test aperture. This conclusion is supported by the results of a recently published numerical simulation. Experimental evidence is presented that suggests that the measured small-scale distortions may have been caused by temperature discontinuities in the splitter-plate boundary layer that fed into the shear layer.

Introduction

THE transmission of a collimated beam of light through a turbulent, variable index-of-refraction flow (caused by density variations, for example) produces a time-varying distortion on the previously planar optical wave front. When the depth of the turbulent region is on the same order as the beam aperture or less, the phenomenon is termed "aerooptics."[1] The high-propagation speed of light relative to practical flow speeds means that the optical beam sees a "slowly" time-varying series of "frozen" index-of-refraction fields. Thus, the aerooptic problem is inherently tied to the dynamics of the flowfield.

These types of optical propagation conditions can be expected to be encountered in airborne optical systems. For such systems, aerooptics produce a significant loss in performance. Dynamic measurements of aerooptical aberrations hold the promise of eventually allowing adaptive-optic correction of the aberrations to restore system performance.[2] To date, dynamic aerooptical measurements have been mostly limited to low-speed flows using dissimilar-index mixing to produce the aberrations. Although these flows have proven to be good for developing new optical diagnostic tools,[3,4] the question of what sort of dynamic aberrations would be produced by a flowfield more representative of a jet-aircraft's optical installation has remained unanswered. To address this question, the Acoustic Research Tunnel (ART) at Arnold Engineering Development Center (AEDC) was modified to produce a weakly compressible shear layer in 1993. Important design features of the facility will be summarized; a more detailed description of the facility may be found in Ref. 5.

The ART facility operates off of bleed air supplied by the AEDC 16T/16S wind-tunnel complex. The shear layer was produced from a ~0.8 Mach high-speed side (velocity, $U_1 \approx 261$ m/s) mixing with a ~0.1 Mach low-speed side ($U_2 \approx 35$ m/s) as shown schematically in Fig. 1. For these tests, the unit Reynolds numbers for the slow and fast streams were 1.4 and 12.7×10^6/m, respectively. Because each stream was supplied from a common plenum, they shared a common total temperature $T_0 \approx 27°$C. The static pressure across the shear layer was constant and equal to the stream-matched static pressure, $p_\infty \approx 0.6$ atm (Ref. 5). These flow conditions can properly be classified as nearly incompressible.[6]

The facility had three observation stations. The first was centered 4.2-cm downstream of the trailing edge of the splitter plate, and the remaining two were spaced 48.3 cm successively downstream. Each station consisted of four viewing windows. Two, 20.32-cm-diam, schlieren-grade windows were on either side of the facility for viewing along the span of the splitter plate or "flow-visualization path" (as shown in Fig. 1). The remaining two windows per station, each 75 mm in diameter, were on the horizontal tunnel walls, that is, top and bottom, to allow optical access normal to the splitter plate (the "aerooptics path"). Notre Dame researchers were invited to make optical wave front measurements in the facility using their then-new wave front sensor, the small-aperture beam technique (SABT). As detailed in Refs. 7 and 8, Hugo et al. successfully obtained the first time-resolved, time series of optical wave fronts for propagation through a compressible shear layer.

The growth rate of a mixing layer is driven by the growth of large-scale, vortex structures.[9,10] This growth rate has been characterized in semi-empirical laws for incompressible mixing layers[11,12] with corrections for compressibility[12–14] as will be summarized. The average vortical roller diameter δ_{viz}, measured from schlieren photographs of compressible shear layers, can be estimated from the following empirical relation reported in the literature[14]:

$$\left(\frac{\delta_{viz}}{x}\right) = C_\delta \frac{(1 - r_u)\left(1 + \sqrt{s}\right)}{1 + r_u\sqrt{s}} \tag{1}$$

where r_u is the velocity ratio U_2/U_1, $s = \rho_2/\rho_1$, and C_δ is a constant ≈ 0.17 for the present convective Mach number. For the AEDC shear layer conditions, Eq. (1) predicts $\delta_{viz} \approx 12.6$ cm at the center of the station 2 aperture, that is, a structure more than twice the size of the 5-cm test aperture. The effect of the aperture is to act as a spatial filter on the measured wave front. The distortion caused by these largest-scale flow structures is, thus, reduced to a time-varying, tilt aberration with a period indicative of the large-scale structure.[15,16] Note that the spatial wavelength of the aberration caused by a compressible shear layer would be expected to correspond to the length of the vortex roller and the braid connecting it to the following roller.[17] This characteristic wavelength Λ, then, would equal the spacing between vortex rollers. Λ can be estimated (on average) by[9,11,18,19]

Presented as Paper 2000-0991 at the AIAA 38th Aerospace Sciences Meeting, Reno, NV, 10–13 January 2000; received 13 March 2000; revision received 25 June 2001; accepted for publication 25 June 2001.

*Research Assistant, Hessert Center for Aerospace Research, Department of Aerospace and Mechanical Engineering, 122 Hessert Center. Senior Member AIAA.

†Professor, Hessert Center for Aerospace Research, Department of Aerospace and Mechanical Engineering, 122 Hessert Center. Associate Fellow AIAA.

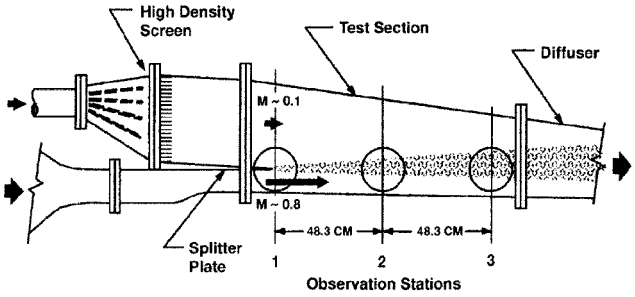

Fig. 1 Schematic of AEDC facility, from Ref. 5.

$$\Lambda/x = C_\Lambda(\delta_{\text{viz}}/x) \tag{2}$$

where C_Λ is an empirical constant. Typical values of C_Λ reported in the literature are from 1.5 (Ref. 9) to 1.95 (Refs. 18 and 19). For an aberrating structure of characteristic size Λ, the wave front aberration temporal frequency would be expected to vary with the structure's convection velocity as

$$f_{\overline{\text{OPL}}} = U_c/\Lambda \tag{3}$$

The large-scale structures' size and convection velocity ($U_c \sim$ 150 m/s) (Ref. 14) would lead one to expect tilt-distortion variation frequencies of $f_{\overline{\text{OPL}}} \sim$ 600–800 Hz.

Hugo et al. employed a posttest, high-pass digital filter to remove signal noise caused by vibration of the test section's optical access windows.[7,8] They conservatively chose their cutoff frequency to minimize the chances of vibrational corruption of the beam-jitter data.[7] The 2–2.5-kHz corner frequency was also chosen because the small measurement aperture already functioned as a spatial filter for any larger-scale structures. In terms of making use of the measured wave front information, moreover, inferred system-performance estimates are ordinarily made after removing tilt over the aperture. Thus, a caveat was pointed out in Ref. 8 that the wave fronts presented there were specifically restricted in their interpretation to the 5-cm test aperture. In Ref. 8, no attempt was made to try to understand the relevant physical cause of the aberrations but rather simply to present the aperture-restricted data; however, now the present authors are interested in understanding the underlying physics and making use of these data to provide an experimental validation point for numerical simulations. These simulations will be used to scale these experimental data to larger aperture and/or other Mach and static pressure conditions. This new objective requires a more careful selection of the high-pass corner frequency to remove the vibration corruption on the one hand but to preserve the largest-scale-structure influences on the other. The purpose of the present investigation, then, was to determine whether the optical distortions due to these large-scale structures could be recovered from the raw data of Refs. 7 and 8.

This paper begins with a short review of the SABT measurement technique, followed by an analysis of the unfiltered beam-jitter vibration data to justify a new digital-filter choice. The resulting wave fronts are then analyzed.

SABT Fundamentals

The SABT is based on the same principles as Hartmann-plate-based wave front sensors (see Refs. 20 and 21). If an aberrated, that is, nonplanar, wave front is broken into small-aperture beams by interrupting its progress with a perforated plate, these beams will propagate in directions normal to the original wave front at the location of the perforation. Measurement of these new beams' displacements at a specific, known distance from the plate provides a direct measurement of the wave front's spatial gradients in the x–z plane of the plate. If the resolution of the perforations is sufficiently high compared to the aberration structure on the wave front, the wave front figure may be constructed by integrating the gradients over the aperture. This wave front figure is usually specified in terms of an optical path length (OPL) as a function of x and z at the particular instant in time that the beam position displacements (relative to their unaberrated locations) were simultaneously measured.[21] Rather than interrupting the wave front with a plate, a number of methods have been employed including the propagation of individual, small-aperture lasers, which then emerge normal to the large-aperture wave front traversing the same medium at the same instant in time.[4] The instantaneous, relative one-dimensional wave front (relative OPL) in the x direction alone can be constructed from measurements of the beam displacement angle or "beam jitter," θ_x, because

$$\text{OPL}(x) = \int_0^x \left(\frac{\text{d OPL}}{\text{d}x}\right) \text{d}x = \int_0^x (-\theta_x)\,\text{d}x \tag{4}$$

Rather than the absolute OPL, one is typically interested in the relative difference in OPL across the aperture or optical path difference (OPD) defined as

$$\text{OPD}(x) = [\text{OPL}(x) - \overline{\text{OPL}}] \tag{5}$$

where the overbar denotes the spatial average over the aperture.

As first asserted by Malley et al.,[22] the optical aberrations imposed by a convecting, optically active turbulent flow must themselves convect through the viewing aperture. If the aberrations were convecting through the aperture unchanged (Taylor's "frozen flow" hypothesis; see Ref. 23), then the normally obtained fine grid of (closely spaced) individual measurements of the wave front derivative, in the form of off-axis, small-aperture-beam displacements, would no longer be required; the wave front could be reconstructed from a time series of off-axis displacements at a single location. This time series could then yield an OPL as a function of time as

$$\text{OPL}(t) = \int_{t_0}^{t} \left[\frac{\text{d OPL}(t)}{\text{d}x}\right] U_c\,\text{d}t \tag{6}$$

where U_c is the $\text{d}x/\text{d}t$ of the convecting wave front aberration. This provides the OPL(t) at position x, the beginning of the (sub)aperture of interest. The spatial OPL over the rest of the aperture follows from Taylor's hypothesis

$$x = -U_c(t - t^*) \tag{7}$$

where t^* is the instant in time at which the spatial OPL is desired. This realization allowed for the first-time-ever measurement of wave fronts at demonstrated rates up to 100 kHz (Refs. 7 and 8). The SABT's high bandwidth made possible the study of optical aberrations caused by propagation through high-speed flows.[7,8]

Implementation of this idea to construct actual wave fronts rather than statistical estimates of the wave front[22] is complicated by the aberrations changing as the turbulence evolves. In addition, U_c not only changes with time, but different turbulent structures convect at different speeds through the aperture, and there are always multiple structures in the viewing aperture at any given time. Furthermore, U_c is not known a priori. The SABT sensor overcomes these complications by using relatively few, multiple probe beams to produce a sparse-detector, high-speed, wave front sensor. From the time series of $\theta_x(t)$ in at least two locations, the convection velocity U_c of the aberrating flow structures between any two beams can be determined using cross correlations of the jitter signals. The SABT method is described in further detail in Refs. 4, 24, and 25.

The experimental wave front data collected at the AEDC facility used the SABT technique and required the use of only two probe beams. The SABT data presented here used a beam spacing $\delta = 2.5$ cm; the rationale for this choice of δ and the resulting wave front uncertainty are detailed in Ref. 8. Detectors measured each beam's streamwise and cross-stream displacement even though this latter measurement could not be used for wave front reconstruction. Details of the AEDC optical bench, beam insertion methods, etc., may be found in Refs. 7 and 8.

Vibrational Noise Removal

Hugo et al. noted that when tunnel 16T was running (but with no air flowing through the ART test section), jitter signals from both detectors "contained identical large amplitude fluctuations ranging from 8 Hz to 2 kHz."[7] This noise was attributed to tunnel vibration.

Dedicated jitter and accelerometer data were acquired to characterize the vibrations to develop a method to remove this noise. Based on these data, Hugo et al. concluded that noise corruption was confined to frequencies below 2.0 kHz. Thus, any noise could be removed by a 2.5-kHz, high-pass, digital filter during data postprocessing without impacting their results (which were already spatially filtered by the 5-cm test aperture).[7,8] A closer look at the vibration data was necessary to justify lowering the corner frequency of the high-pass filter. The analysis to be described is presented with the detailed supporting data in Ref. 17.

Hugo et al. acquired vibrational data using two accelerometers attached to the tunnel's outside surface. The station 1 accelerometer was mounted on the bottom of the tunnel approximately 1.27-cm downstream of aerooptic window 1; the station 2 accelerometer was similarly mounted approximately 2.54-cm upstream of the second aerooptic window. The accelerometer signals were acquired simultaneously with beam jitter data during three dedicated runs.[7,8] The beam-jitter data were obtained by passing two SABT-type probe beams with a separation $\delta = 1.27$ cm through the station 1 aerooptic windows. As a baseline case, vibration data were acquired while AEDC tunnel 16T was off. The accelerometer data showed that there was negligible vibration for this 16T-off/air-off case.

The second set of vibration data was acquired with 16T operating but with no flow through the ART (16T-on/air-off case). In this case, any measured jitter must have been due to tunnel vibration only because there was no flow to produce an aerooptic distortion. An order of magnitude increase in accelerometer vibration energy over the 16T-off/air-off case occurred at this condition at frequencies below ~2000 Hz, although the vibrations measured by the accelerometers were still fairly small. A similar, although less pronounced, increase was also apparent in the jitter signals at these frequencies. Three of the four jitter signals showed a small, broad peak at ~1250 Hz. Any vibration would be expected to affect both beams or both accelerometers together, producing high coherence between the signals; the high phase speeds expected in solids such as the windows or the (metal) tunnel walls, meanwhile, would lead to approximately zero phase difference between them. The coherence and phase angles between upstream and downstream signals for the 16T-on/air-off case behaved in this way. The coherence of the beam jitter data was a particularly good measure of this behavior (high coherence/zero phase) over the entire range of frequencies between 0 and 5000 Hz. This can be attributed to the close spacing of the beams and to the sensitivity of the instrument (small changes in window position were magnified by the ~3-m distance the beam traveled from the window to the detector).

The final set of vibration data was acquired with the ART running (16T-on/air-on case). The overall vibration level increased significantly for this case relative to the two air-off cases. The jitter spectra had only one major peak below 400 Hz, which was likely due to the 16T vibration; the jitter spectra above ~400 Hz had a broadband character with no appreciable rolloff. The accelerometers measured significant vibrations with narrow peaks at ~200 and 500 Hz and a large broad series of peaks from ~900 to 1300 Hz. Surprisingly, there were no obvious peaks in the jitter spectra corresponding to those in the accelerometer spectra. Because the jitter spectra included both vibrations and aerooptical distortions, this lack of distinct peaks suggests that the vibrational portion of the beam-jitter signal was less significant than the aerooptical portion at these frequencies.

For the 16T-on/air-on case, the coherence magnitudes and phase behavior did not change significantly for the accelerometer signals, but the addition of aerooptical distortion to the jitter signal produced coherence and phase behavior that was more irregular than the 16T-on/flow-off case. For the jitter-coherence peaks at frequencies below 500 Hz, the phase angle was approximately 0 deg. This suggests that disturbances below 500 Hz were caused by vibrations. For coherence peaks at frequencies above 500 Hz, however, the phase angle was generally nonzero and gradually increased with frequency. This was especially apparent in the cross-stream signal. Such nonzero phase angles demonstrate a time difference between when an event was measured by each sensor. Because vibrational phase speeds in glass and steel are on the order of 6000 m/s (Ref. 26), a more likely cause of these delays would be aerooptical disturbances convecting between the beams.

Another way to assess which frequencies would be susceptible to vibrational corruption would be to examine the beam-jitter coherence/phase behavior at different beam separations. (Recall that accelerometer data were only acquired for the three cases described and so they were unavailable for other beam spacings.) Because any vibration would presumably disturb an entire window, one might expect high coherence/zero phase at the affected frequencies to be independent of beam spacing. Furthermore, one might expect that any significant vibration transmitted via the tunnel walls would be common to the aerooptic-path windows at both stations 1 and 2. When coherence and phase angle for the station 1 window for beam separations $\delta = 25.4$ and 38.1 mm were examined, a common region of high coherence and near-zero phase angle was found to extend from $f \approx 100$ to ~700 Hz. This was particularly clear in the cross-stream jitter component. In fact, similar results were found when the analysis was applied to the station 2 data. For the station 2 case, moreover, the region of near-zero phase appeared to end by $f = 500$ Hz. These data suggested that the high-pass filter's corner frequency might reasonably be reduced to ~500–700 Hz.

To further investigate what the proper filter setting would be, a series of wave front reconstructions were performed on a single dataset from each tunnel station. During this series, the high-pass filter cutoff frequency was varied. Each high-pass filter was a third-order, zero-phase-shift Butterworth filter applied using MATLAB® (as described in Ref. 7). The filter's corner frequencies were chosen to progressively pass individual peaks in the accelerometer power spectra: 2 kHz (Ref. 7 case), 1.2 kHz (between expected structure size and largest accelerometer peak), 750 Hz, and 0 Hz (unfiltered). Because station 1 began only 3.575-cm downstream of the splitter plate trailing edge, only very small structures would be present due to an initial shear layer rollup or to aberrating disturbances fed into the shear layer from the splitter-plate boundary layer. Regardless of their cause(s), these structures' small spatial wavelengths correspond to much higher frequencies than those of the vibrations. Thus, low-frequency structures can be attributed to tunnel vibration. The resulting OPD time series for station 1 are shown in Fig. 2. For the unfiltered case (Fig. 2d), a fairly large, very-low-frequency tilt corrupts the entire wave front measurement. Once the filter's corner frequency is raised to 750 Hz or above (Figs. 2a–2c), however, there is no evidence of a low-frequency tilt. This suggests that jitter signal energy below 750 Hz can be attributed to vibration, as suggested by the results of the coherence/phase study.

When the same filter settings are applied to station 2 data, the OPD time series shown in Fig. 3 result. When the 2-kHz filter of Ref. 7 is applied (Fig. 3a), periods displaying large-scale structures were intermittent (cf., time equal to 2–4.5 ms) and significant periods existed with only small-scale structures similar to those seen in the station 1 OPDs (cf., time equal to 0–2 ms) as noted by Hugo et al.[8] When the filter is reduced to 1.2 kHz (Fig. 3b), large-scale structures appear in the regions that earlier had no large structures. These structures correspond to a frequency of ~1.3 kHz. When the filter's corner frequency is reduced further to 750 Hz (Fig. 3c), no new structures appear. In fact, the only change is a slight amplification in the earlier seen large structures due to the larger separation between the filter's corner frequency and the structure frequency. When no filter is used (Fig. 3d), however, a lower-frequency vibration again begins to corrupt the data, as was the case at station 1: for $t > 3.5$ ms, a large, low-frequency tilt dominates the signal. Based on the results of these filter studies and the coherence data at both stations, the 750-Hz high-pass filter was chosen to minimize vibrational noise in the data without removing frequencies corresponding to flow-structure sizes predicted using equations found in the literature.

Results

Evidence of Large-Scale Structures

With the lowering of the high-pass filter cutoff frequency to 750 Hz, the station 2 OPDs are clearly dominated by large-scale structures. As was shown in Fig. 3c, the effect of including these large-scale structures is significant: OPD_{rms} increased approximately 60% as the high-pass filter cutoff was lowered from 2 kHz

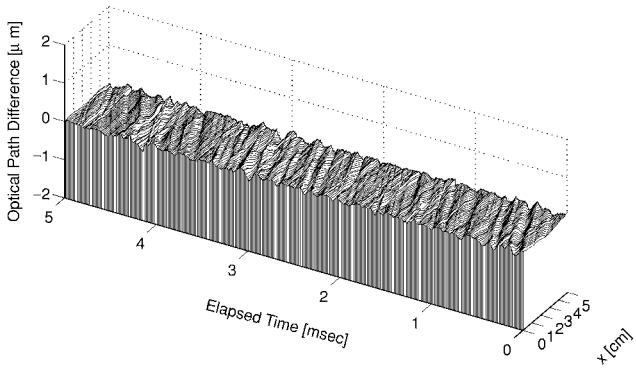

a) High-pass filter: 2000 Hz; $\bar{U}_c = 155.15$ m/s, $\bar{M}_c = 0.456$, and $OPD_{rms} = 0.0453$ μm ≈ 0.0716 waves

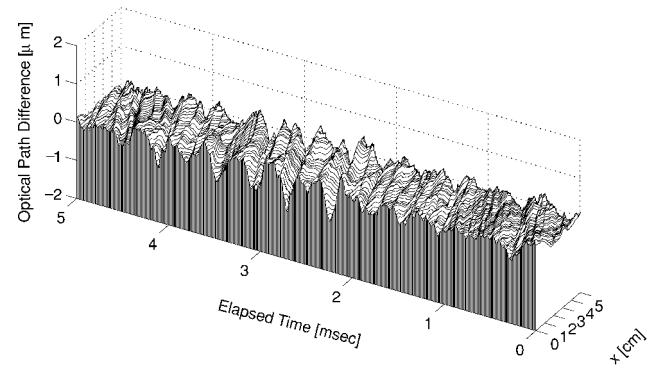

a) High-pass filter: 2000 Hz; $\bar{U}_c = 166.22$ m/s, $\bar{M}_c = 0.489$, and $OPD_{rms} = 0.167$ μm ≈ 0.265 waves

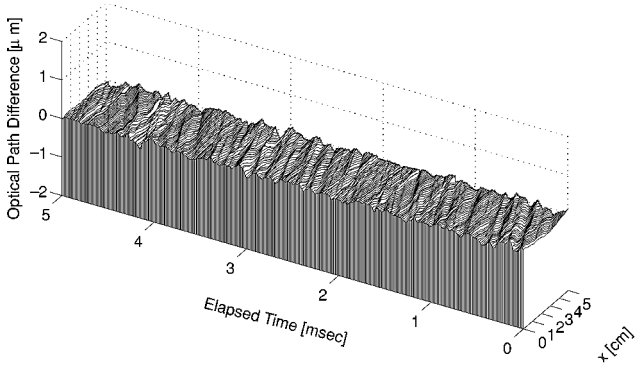

b) High-pass filter: 1200 Hz; $\bar{U}_c = 154.27$ m/s, $\bar{M}_c = 0.454$, and $OPD_{rms} = 0.0505$ μm ≈ 0.0799 waves

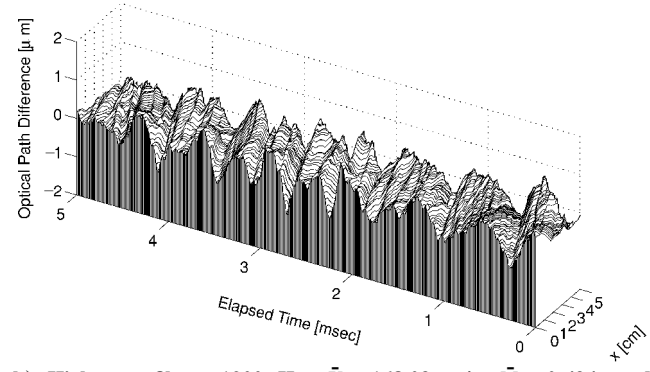

b) High-pass filter: 1200 Hz; $\bar{U}_c = 168.03$ m/s, $\bar{M}_c = 0.494$, and $OPD_{rms} = 0.230$ μm ≈ 0.364 waves

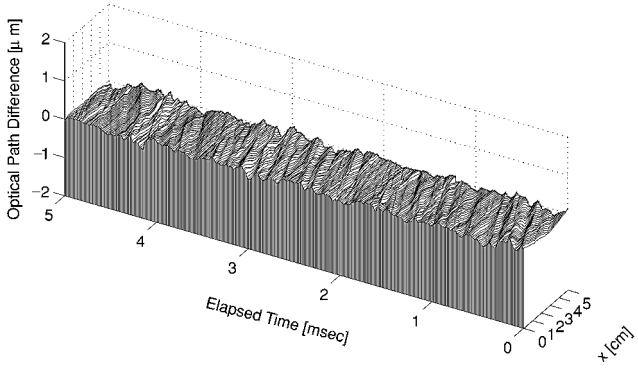

c) High-pass filter: 750 Hz; $\bar{U}_c = 154.16$ m/s, $\bar{M}_c = 0.453$, and $OPD_{rms} = 0.0573$ μm ≈ 0.0905 waves

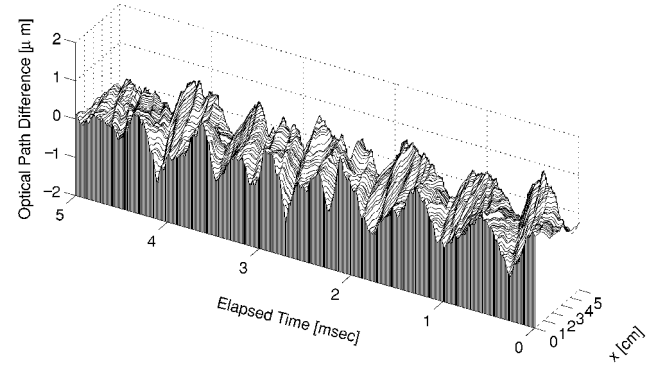

c) High-pass filter: 750 Hz; $\bar{U}_c = 170.47$ m/s, $\bar{M}_c = 0.501$, and $OPD_{rms} = 0.274$ μm ≈ 0.434 waves

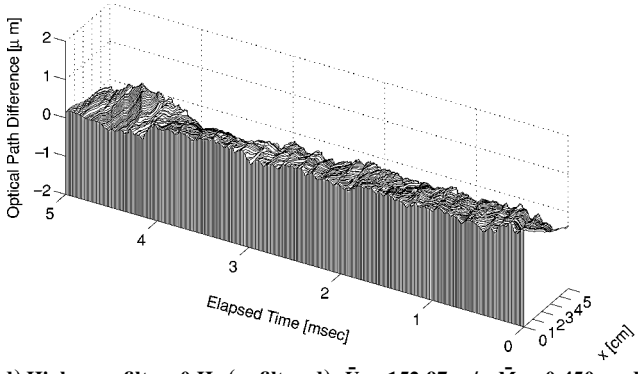

d) High-pass filter: 0 Hz (unfiltered); $\bar{U}_c = 152.97$ m/s, $\bar{M}_c = 0.450$, and $OPD_{rms} = 0.2283$ μm ≈ 0.3610 waves

Fig. 2 Effect of varying posttest, high-pass filter setting from 2000 to 0 Hz on resulting wave front reconstructions, computed convection velocity, and OPD_{rms}. AEDC station 1, $\delta = 2.5$ cm, and $\lambda = 632.8$ nm.

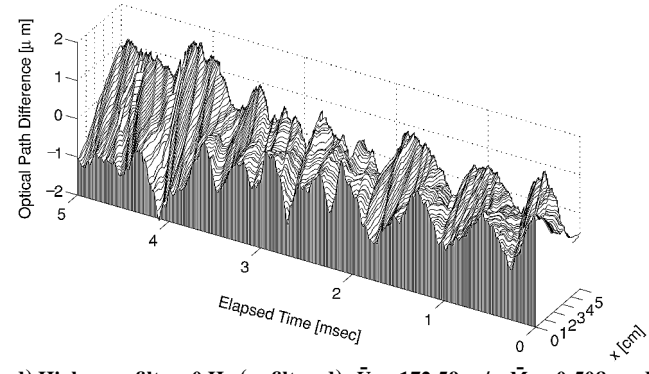

d) High-pass filter: 0 Hz (unfiltered); $\bar{U}_c = 172.59$ m/s, $\bar{M}_c = 0.508$, and $OPD_{rms} = 0.424$ μm ≈ 0.669 waves

Fig. 3 Effect of varying posttest, high-pass filter setting from 2000 to 0 Hz on resulting wave front reconstructions, computed convection velocity, and OPD_{rms}. AEDC station 2, $\delta = 2.5$ cm, and $\lambda = 632.8$ nm.

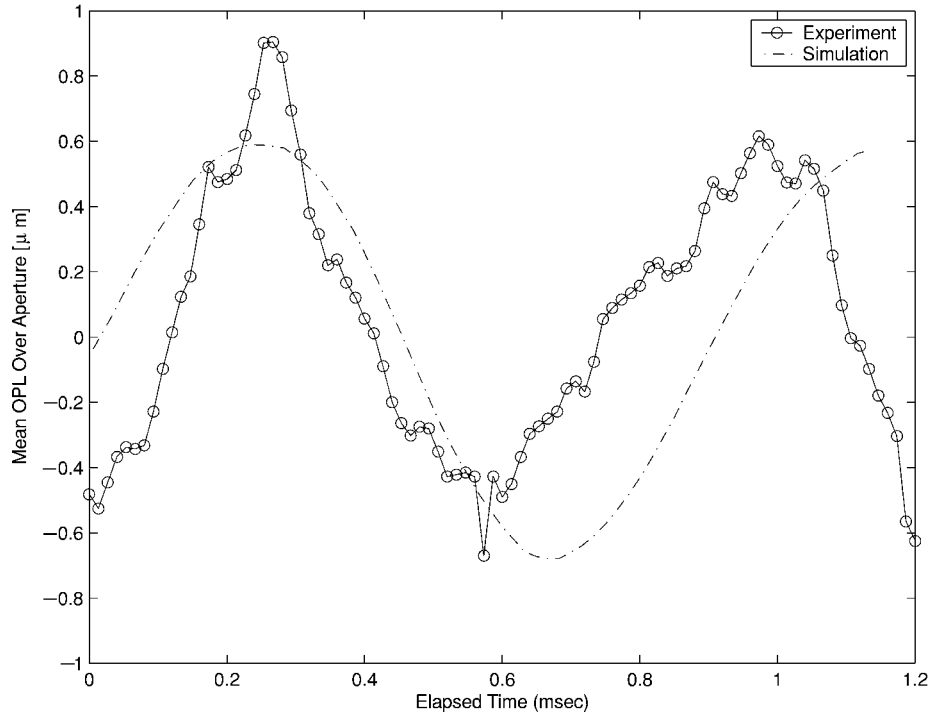

Fig. 4 Variation of $\overline{\text{OPL}}$ removed in OPD calculation with time for experimental reconstruction (δ = 2.5 cm, high-pass filter = 750 Hz) and numerical simulation ($\delta_t/2$ = 8.626 mm from Ref. 16), AEDC station 2.

to 750 Hz. The wave front time series shown in Fig. 3c is fairly representative of the station 2 data for this aperture setting. The OPD_{rms} for all 186 ms of data acquired for this aperture and high-pass filtered at 750 Hz is 0.242 μm or $\approx$0.383 waves (based on the HeNe laser wavelength $\lambda = 632.8$ nm).

Another indication of large-scale structures can be seen in the time-varying piston aberration, $\overline{\text{OPL}}$, removed at each time step in the computation of OPD. For instance, one could model a shear layer vortex roller as a circular cylinder of fluid having a different density, that is, index of refraction, than the surrounding fluid and its axis aligned in the spanwise direction. Consider the optical aberration this cylinder would create as it crossed a much smaller optical aperture. As the downstream edge of the structure entered the aperture, there would be negligible distortion; the distortion would gradually increase, reaching a maximum when the beam passed through the center of the structure; finally, the distortion would again decrease to a negligible level.[4,25] As the structure convected across this (small) aperture, most of the distortion amplitude would be contained in the instantaneous mean OPL across the aperture [the $\overline{\text{OPL}}$ that is removed by the OPD calculation, cf., Eq. (5)]. In fact, the experimental $\overline{\text{OPL}}$ varies in just this way, as shown in Fig. 4. Note the size of $\overline{\text{OPL}}$: Over a larger aperture, this optical piston component would result in a significant increase in the overall OPD.

Because the wave front data were only acquired over a limited aperture (5 cm), the large-scale structures appear as time-varying tilt aberrations as already discussed. Further extrapolation of the wave front data to an aperture large enough to see the structure size would be unreliable because turbulent structures continue to evolve as they move downstream; however, an order-of-magnitude estimate of the large-scale structure size is still possible. An estimate of the structure size follows from Eq. (3). A typical period of one of the $\overline{\text{OPL}}$ structures in Fig. 4 is $\approx$0.72 ms or $f_{\overline{\text{OPL}}} \approx 1415$ Hz. From the wave front reconstruction process, the average convection velocity during that cycle was $\overline{U_c} = 160$ m/s, which gives an estimated structure size $\Lambda \approx 11.3$ cm. Through Eq. (2), this value of Λ would correspond to an instantaneous δ_{viz} of 5.8–7.5 cm (depending on the choice of C_Λ). This also compares well with the 7–9 cm structure diameter measured in the holographic interferogram shown in Fig. 5. Whereas these diameter estimates are considerably smaller than the average vortical roller diameter predicted by Eq. (1) for the center of the station 2 aperture ($\delta_{viz} \approx 12.6$ cm), it should be remembered that Eq. (1) predicts an average value only. Because a shear layer grows

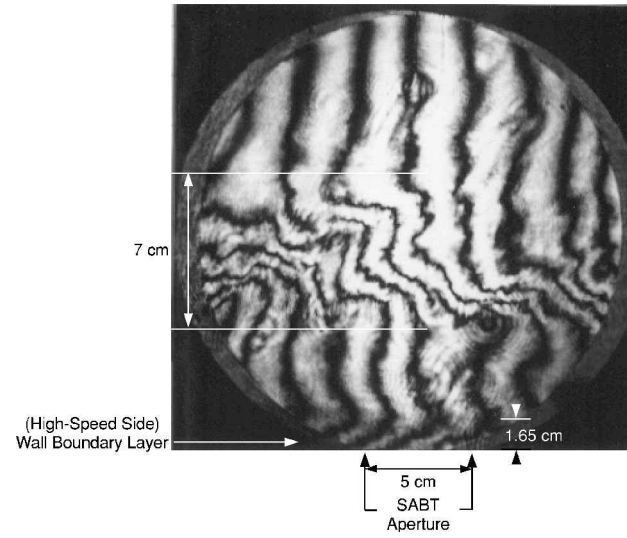

Fig. 5 AEDC station 2 holographic interferogram (flow-visualization path), from Ref. 5.

by the rollup and subsequent pairing of vortices, instantaneous vortex rollers could be significantly smaller than the Eq. (1) prediction if a particular pairing event did not occur until downstream of the aperture.[27] It seems likely, therefore, that the largest-scale, distorting flow structures correspond to the vortex rollers and their connecting braids observed in compressible shear layers.[12,14]

A final argument that these tilt aberrations are caused by large-scale, compressible flow structures comes from comparison of these data to the recently published results of a numerical simulation of this flowfield.[16] In that study, a discrete vortex method was used to produce a first-order approximation to the instantaneous, unsteady velocity field in a weakly compressible shear layer. From this known velocity field, the resulting index-of-refraction field and wave front aberrations were computed. The numerical result for the 5-cm aperture compares well to the (replotted) experimental result, as shown in Fig. 6. The dominant cause of the numerical simulation's distortions was the unsteady pressure field, which mechanically balances the

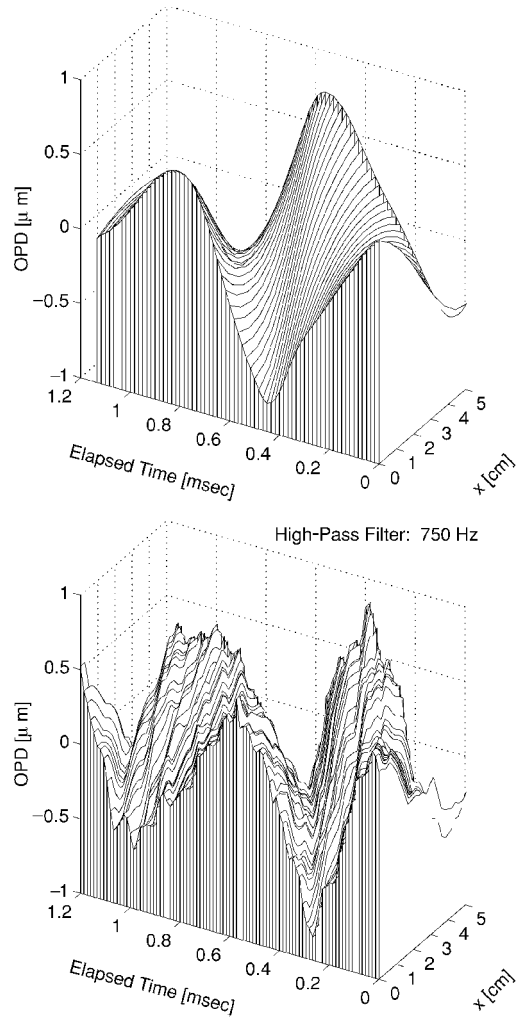

Fig. 6 AEDC station 2 numerical simulation: $\delta_i/2 = 8.626$ mm (top) (from Ref. 16) and experimental wave front reconstruction: beam separation, $\delta = 2.5$ cm, high-pass filter = 750 Hz (bottom).

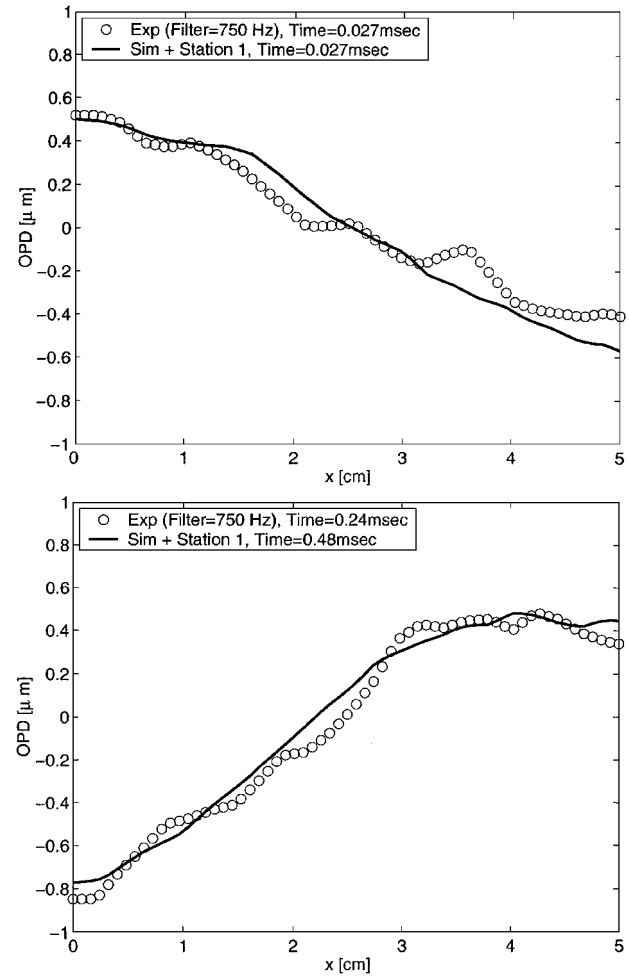

Fig. 7 Comparison of individual AEDC station 2 experimental wave fronts (from Fig. 6) with numerical simulation and superimposed station 1 wave fronts (from Fig. 10) at corresponding time steps.

streamline curvature produced by large-scale, vortical structures.[16] A more quantitative comparison of these data is shown in Fig. 7 for two sets of the individual wave fronts taken from corresponding time steps, that is, accounting for the ~0.24–ms difference in the experimental and numerical wave fronts' temporal wavelengths, which can be attributed to the inability to completely match the shear layers' initial conditions. In both cases shown in Fig. 7, the simulation does a good job of capturing the low-order shape of the wave front. Only at the smallest scales are differences between each set of wave fronts greater than the 12% uncertainty of the experimental data[8]; these differences coincide with smaller-scale structures that were not captured by the simulation and so were overlaid later. (The simulation wave fronts in Fig. 7 are actually taken from results shown subsequently, explained in the next section.) Similarly, the $\overline{\text{OPL}}$ removed from the numerical simulation to match the experimental aperture also compares well in amplitude and phase with the experimental result as shown in Fig. 4, albeit with the aforementioned difference in temporal wavelength. The similarity of the numerical and experimental results in Figs. 4, 6, and 7 argues that the measured aerooptical tilt aberrations are produced by the largest-scale flow structures. Note that, if these larger structures are present, the OPD peak-to-peak error over a large aperture (like the 20-cm aperture of the original Ref. 16 simulation) would be considerably larger than the approximately 0.1–0.25 waves reported for the station 2 aperture in Ref. 8.

In addition to the large-scale structures, smaller-scale distortions are also present in the station 2 wave fronts. The size and structure of these fine-scale distortions are reminiscent of the station 1 wave front aberrations and are examined in next section.

Small-Scale Structures

Wave fronts measured at both stations 1 and 2 feature small-scale distortions that are shown most clearly in the station 1 wave fronts of Fig. 2c. With the available flow diagnostic data essentially limited to the pulsed-holographic-interferometry results presented in Ref. 5, the cause(s) of these fine-scale optical distortions cannot be determined with certainty; however, the wave front and jitter data can be used to suggest a possible explanation for these distortions.

For the station 1 aberrations to be caused by a vortex rollup of the shear layer as was discussed for the station 2 wave fronts of the last section, the initial rollup would need to occur by the beginning of the SABT aperture, 3.575 cm downstream of the splitter plate trailing edge. This initial rollup occurs when the shear layer momentum thickness θ grows to approximately three times the wavelength λ_n of the shear layer's most unstable frequency mode f_n (Ref. 27). This most unstable mode can be estimated from the momentum thickness of the high-speed stream at the splitter plate trailing edge, θ_0 (Refs. 27 and 28). For the presumed-turbulent, AEDC splitter-plate boundary layer, $\theta_0 \leq 0.38$ mm would be required for rollup by $x = 3.575$ cm (Ref. 27); if a $\frac{1}{7}$-power law velocity profile is assumed, this corresponds to a boundary-layer thickness $\delta_{99\%} \leq 3.92$ mm (Ref. 29). An estimate of $\delta_{99\%}$ can also be made for the AEDC shear layer from the station 1 holographic interferogram shown in Fig. 8. Large fringe shifts mark the high-speed splitter-plate boundary layer, which maintains its approximate thickness and character as it progresses downstream, at least to the center of the SABT measurement aperture. At the splitter trailing edge, $\delta_{99\%} \approx 6.5$ mm, suggesting the initial shear layer rollup would occur near the center of the SABT test aperture. Indeed, the character of the fringe shifts changes downstream of the center of the SABT aperture, suggesting such a rollup has occurred. Close inspection of Fig. 2c, however,

shows the largest wave front aberrations to have a spatial extent of 1–2 cm and to be already present at the beginning of the SABT aperture. Because Fig. 8 shows no noticable change in shear layer structure between the splitter-plate trailing edge and the start of the SABT aperture, it is highly unlikely that the measured distortions were produced by shear layer rollup. Thus, the small-scale aberrations are likely formed by a different mechanism than the large-scale distortions that dominate the station 2 wave fronts.

Another indication of the cause of the fine-scale distortions comes from examining the jitter signals themselves. A sample of these signals are shown for the upstream detector in Fig. 9. The cross-stream beam-jitter amplitude is of the same order as the streamwise component. Wissler and Roshko found that this sort of jitter behavior corresponds to the three-dimensional turbulence that occurs downstream of so-called "mixing transition."[30] [For a shear layer produced from laminar splitter-plate boundary layers, mixing transition occurs for x/θ_0 of at least 150 (Ref. 31).] Because the upstream beam is located at the beginning of the aperture (where $x/\theta_0 \approx 60$ only), already turbulent flow must be entering the station 1 aperture. These structures convect through the aperture at $\sim U_c$, as is clearly shown by Fig. 2c. Such turbulent structures could form in the compressible boundary layer on the high-speed side of the splitter plate and/or on the observation window in the tunnel wall.[32] Both of these distortion sources are apparent in the holographic interferogram of Fig. 8.

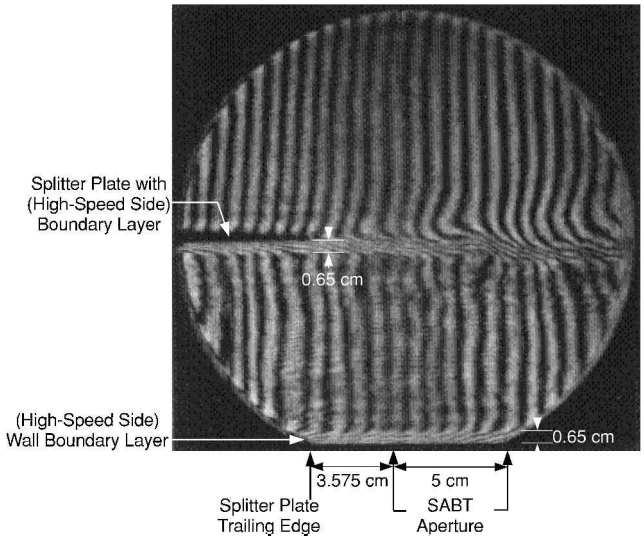

Fig. 8 AEDC station 1 holographic interferogram (flow-visualization path), from Ref. 5.

A possible mechanism for creating optical distortions in a turbulent boundary layer is by adiabatic heating. The large velocity gradient (0.8 Mach to zero) over the small thickness of the turbulent boundary layer could create dissimilar-temperature turbules by the adiabatic heating, which would accompany the local flow deceleration. These dissimilar-temperature turbules would have a spatial size that could be a significant fraction of the turbulent boundary-layer thickness. The characteristic size of these structures appears to be $\sim$1–2 cm (cf., Fig. 2c). Once created, these turbules would likely convect at approximately the shear layer convection speed U_c (for the splitter-plate boundary-layer-caused scenario) or $\approx U_1/2 \sim U_c$ (window boundary-layer case).

Once created and convecting, the next question is how long would such structures persist? If the turbules were convecting along at $U_c \approx 150$ m/s, the convection time from the splitter plate trailing edge to the center of station 2 would be approximately 3 ms. The heat transfer time constant τ for one of these turbules can be estimated by modeling it as a hot sphere of fluid, initially at a constant temperature, conducting heat to the lower-temperature surrounding fluid. As a fastest case, the surrounding fluid can be considered as a large reservoir that conducts the heat away fast enough that the temperature at the surface of the sphere remains at the reservoir temperature. The temperature field within the sphere is governed by the heat-diffusion equation; its solution is a Fourier sine series for which each mode has a different τ (Refs. 33 and 34). For a 1–2 cm diam sphere at the AEDC conditions, a rapid reduction in the initial temperature gradient would occur near the sphere's edge (due to the fast decay of higher-order modes); however, in the absence of external shear, neither the overall temperature nor size of the sphere, that is, effective radius, would significantly change, even in the time required to convect to station 3. The time constant of the lowest-order modes was found to be $\tau \sim 56$ ms, more than 15 times the convection timescale.[17] Because this thermal-diffusion time constant is an order of magnitude larger than the convective timescale, it is reasonable to assume a thermal turbule could retain its dissimilar index as it convected through the test section.

No matter how a thermal turbule was originally formed, whether in the splitter plate or window boundary layer, its effect would be to superimpose a small-scale distortion on the wave front. In the first

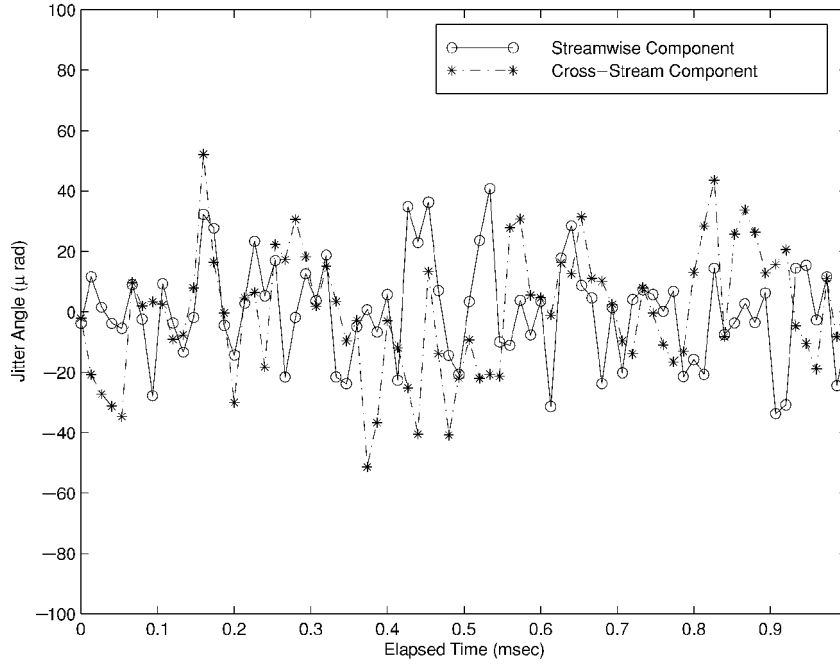

Fig. 9 AEDC station 1 beam-jitter signals: upstream detector (United Detector Technologies Model 301 amplifier) (frequency-compensated signals, high-pass filtered at 750 Hz).

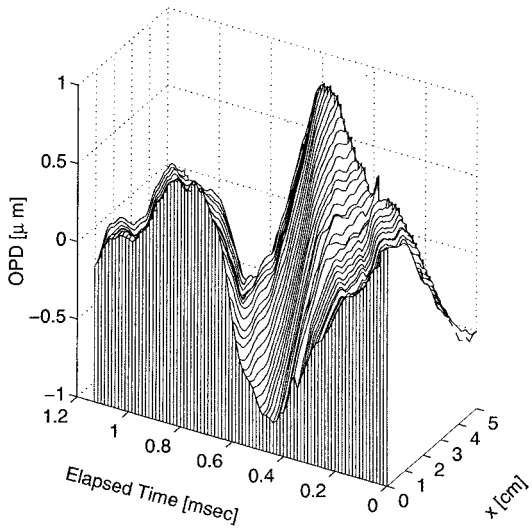

Fig. 10 AEDC station 2 wave fronts produced by superposition of numerical simulation (Fig. 6) and station 1 experimental data (Fig. 2c), from Ref. 16.

case, the small flow structures would be expected to be entrained into the mixing layer and remain essentially unchanged; in the second case, the boundary layer on the window at station 2 (now thicker than it was at station 1) would be superimposed on the mixing layer distortion. Both of these cases suggest that the overall OPD might be modeled as a superposition of a large-scale aberration associated with shear layer rollup and small-scale aberrations similar to those measured at station 1. To investigate this possible distortion mechanism, the aberrations shown in Fig. 2c were linearly superimposed on the numerical results of Fig. 6 to produce Fig. 10. The simulation wave fronts in Fig. 10 do have comparable structure amplitudes and wavelengths to the experimental wave fronts of Fig. 6 as was clearly shown in Fig. 7. The poor amplitude/position matching of the small-scale aberrations in Fig. 7 would be expected because no attempt was made to link individual window 1 aberrations with those of similar scale measured in the window 2 aperture. Thus, it seems at least feasible that the small-scale distortions were caused by temperature structures that have been entrained into the larger-scale swirling eddies of the shear layer and/or due to the turbulent boundary layer on the tunnel window.

Understanding the physical mechanisms creating these wave front aberrations is ultimately important for optical-system design applications. If the measured OPD structures were caused solely by the shear layer rollup and concomitant pressure fields superimposed on a dirty temperature field (fed into the shear layer at the splitter plate), station 2's 5-cm test aperture could lead one to associate these aberrations with the largest-scale flow structures. Thus, subsequent estimates of the dominant OPD wave numbers and temporal frequencies for a large-aperture case, that is, >5 cm, would be overpredicted if the Ref. 8 data were used directly. Such an overprediction would cause a similar overprediction of the required bandwidth to accomplish adaptive-optical correction for a compressible shear layer. Moreover, if the measured station-2 OPDs were caused by such a superposition, the small-scale portion of the aberration might be reduced or eliminated by a special treatment, for example, suction removal, of splitter plate and window boundary layers. The bandwidth needed for adaptive-optical corrections of the remaining, large-structure-caused aberrations might then be reduced from 6 to 1.5 kHz. Another dedicated experiment similar to the AEDC test is required to resolve these issues. Such a test would determine the condition of the splitter plate and tunnel wall boundary layers upstream of the shear layer.

Conclusions

Hugo et al. successfully obtained the first time-resolved, time series of optical wave front measurements in the AEDC compressible shear layer facility.[7,8] Their choice of a 2.5-kHz, high-pass digital filter to remove vibrational noise from their jitter signals, while appropriate for the 5-cm test aperture, removed the optical distortions created by the largest-scale flow structures that affect larger-aperture optical-system performance. A more detailed examination of vibration and wave front data justified reducing the high-pass filter setting from 2500 to 750 Hz. With this lower filter setting, clear evidence of large-scale structures was present in AEDC-station-2 OPD time-series data. These large-scale aberrations appear to be comparable in size to the vortices created during shear layer rollup and match the character and amplitude of those predicted by a recent numerical simulation.[16] The underlying flow structures would also produce much larger overall OPDs than those presented in Ref. 8. Because typical airborne telescopes and laser systems use apertures much larger than the 5-cm aperture tested at AEDC, significant optical degradation could result.

A possible mechanism was suggested to explain smaller-scale distortions observed in both the station 1 and station 2 wave fronts. If this mechanism proves to be correct, the overall wave front might be modeled as a superposition of large- and small-scale distortions. In fact, a superposition of the experimentally measured station 1 wave fronts on a numerical simulation of the large-scale distortions produces wave fronts that closely resemble those measured at station 2. These small-scale distortions might be removable by boundary-layer suction, for example.

An experimental dataset has now been obtained and reduced for light propagation through a compressible shear layer. Analytical models of the compressibility mechanism and scaling laws can now be explored and validated against this dataset.

Acknowledgments

These efforts were sponsored by the Air Force Office of Scientific Research, Air Force Material Command, U.S. Air Force, under Grant F49620-97-1-0489. The U.S. Government is authorized to reproduce and distribute reprints for Governmental purposes notwithstanding any copyright notation thereon.

References

[1]Gilbert, K. G., "Overview of Aero-Optics," *Aero-Optical Phenomena*, edited by K. G. Gilbert and L. J. Otten, Vol. 80, Progress in Astronautics and Aeronautics, AIAA, New York, 1982, pp. 1–9.

[2]Cicchiello, J. M., and Jumper, E. J., "Far-Field Optical Degradation due to Near-Field Transmission Through a Turbulent Heated Jet," *Applied Optics*, Vol. 36, No. 25, 1997, pp. 6441–6452.

[3]Neal, D. R., O'Hern, T. J., Torczynski, J. R., Warren, M. E., Shul, R., and McKechnie, T. S., "Wavefront Sensors for Optical Diagnostics in Fluid Mechanics: Application to Heated Flow, Turbulence and Droplet Evaporation," *Optical Diagnostics in Fluid and Thermal Flow*, edited by S. S. Cha and J. D. Trollinger, Vol. 2005, SPIE—The International Society of Optical Engineering, Bellingham, WA, 1993, pp. 194–203.

[4]Jumper, E. J., and Hugo, R. J., "Quantification of Aero-Optical Phase Distortion Using the Small-Aperture Beam Technique," *AIAA Journal*, Vol. 33, No. 11, 1995, pp. 2151–2157.

[5]Havener, G., and Heltsley, F., "Design Aspects and Preliminary Holographic-PIV Measurements for a Subsonic Free Shear Layer Flow Channel," AIAA Paper 94-2550, June 1994.

[6]Smits, A. J., and Dussauge, J.-P., *Turbulent Shear Layers in Supersonic Flow*, American Inst. of Physics, Woodbury, NY, 1996, pp. 80–90, 115–160.

[7]Hugo, R. J., Jumper, E. J., Havener, G., and Stepanek, C., "Time-Resolved Aero-Optical Measurements of a Wavefront Aberrated by a Compressible Free Shear Layer," AIAA Paper 95-1979, June 1995.

[8]Hugo, R. J., Jumper, E. J., Havener, G., and Stepanek, C., "Time-Resolved Wave Front Measurements Through a Compressible Free Shear Layer," *AIAA Journal*, Vol. 35, No. 4, 1997, pp. 671–677.

[9]Brown, G. L., and Roshko, A., "On Density Effects and Large Structure in Turbulent Mixing Layers," *Journal of Fluid Mechanics*, Vol. 64, No. 4, 1974, pp. 775–816.

[10]Winant, C. D., and Browand, F. K., "Vortex Pairing: The Mechanism of Turbulent Mixing-Layer Growth at Moderate Reynolds Number," *Journal of Fluid Mechanics*, Vol. 63, No. 2, 1974, pp. 237–255.

[11]Dimotakis, P. E., and Brown, G. L., "The Mixing Layer at High Reynolds Number: Large Structure Dynamics and Entrainment," *Journal of Fluid Mechanics*, Vol. 78, 1976, pp. 535–560.

[12]Hall, J. L., Dimotakis, P. E., and Rosemann, H., "Experiments in Nonreacting Compressible Shear Layers," *AIAA Journal*, Vol. 31, No. 12, 1993, pp. 2247–2254.

[13]Papamoschou, D., and Roshko, A., "Observations of Supersonic Free Shear Layers," AIAA Paper 86-0162, Jan. 1986.

[14]Papamoschou, D., and Roshko, A., "The Compressible Turbulent Shear Layer: An Experimental Study," *Journal of Fluid Mechanics*, Vol. 197, 1988, pp. 453–477.

[15]Cassady, P. E., Birch, S. F., and Terry, P. J., "Aero-Optical Analysis of Compressible Flow over an Open Cavity," *AIAA Journal*, Vol. 27, No. 6, 1989, pp. 758–762.

[16]Fitzgerald, E. J., and Jumper, E. J., "Further Consideration of Compressibility Effects on Shear Layer Optical Distortion," AIAA Paper 99-3617, June 1999.

[17]Fitzgerald, E. J., "The Shear Layer Compressibility Mechanism and Its Role in Creating Aero-Optical Distortions," Ph.D. Dissertation, Aerospace and Mechanical Engineering Dept., Univ. of Notre Dame, Notre Dame, IN, April 2000.

[18]Koochesfahani, M. M., Catherasoo, C. J., Dimotakis, P. E., Gharib, M., and Lang, D. B., "Two-Point Laser Doppler Velocimetry Measurements in a Plane Mixing Layer," *AIAA Journal*, Vol. 17, No. 12, 1997, pp. 1347–1351.

[19]Dimotakis, P. E., "Two-Dimensional Shear Layer Entrainment," *AIAA Journal*, Vol. 24, No. 11, 1986, pp. 1791–1796.

[20]Malacara, D., *Optical Shop Testing*, Wiley, New York, 1978, Chap. 10, pp. 323–345.

[21]Geary, J. M., *Introduction to Wavefront Sensors*, Vol. TT18, Tutorial Texts in Optical Engineering, Society of Photo-Optical Instrumentation Engineers (SPIE), Optical Engineering Press, Bellingham, WA, 1995, pp. 13–20, 89–94.

[22]Malley, M., Sutton, G. W., and Kincheloe, N., "Beam-Jitter Measurements of Turbulent Aero-Optical Path Differences," *Applied Optics*, Vol. 31, No. 22, 1992, pp. 4440–4443.

[23]Hinze, J. O., *Turbulence*, 2nd ed., McGraw–Hill, New York, 1975, pp. 46, 47.

[24]Hugo, R. J., and Jumper, E. J., "Experimental Measurement of a Time-Varying Optical Path Difference by the Small-Aperture Beam Technique," *Applied Optics*, Vol. 35, Aug. 1996, pp. 4436–4447.

[25]Hugo, R. J., "Quantifying the Spatio-Temporal Effects of Optically-Active Turbulent Flowfields on a Coherent Optical Wave," Ph.D. Dissertation, Aerospace and Mechanical Engineering Dept., Univ. of Notre Dame, Notre Dame, IN, April 1995.

[26]Kinsler, L. E., Frey, A. R., Coppens, A. B., and Sanders, J. V., *Fundamentals of Acoustics*, Wiley, New York, 1982, p. 461.

[27]Ho, C. M., and Huerre, P., "Perturbed Free Shear Layers," *Annual Review of Fluid Mechanics*, Vol. 16, 1984, pp. 365–424.

[28]Ho, C. M., and Huang, L. S., "Subharmonics and Vortex Merging in Mixing Layers," *Journal of Fluid Mechanics*, Vol. 119, 1982, pp. 443–473.

[29]Schlichting, H., *Boundary-Layer Theory*, 7th ed., McGraw–Hill, New York, 1979, pp. 636–639.

[30]Wissler, J. B., and Roshko, A., "Transmission of Thin Light Beams Through Turbulent Mixing Layers," AIAA Paper 92-0658, Jan. 1992.

[31]Roshko, A., "The Mixing Transition in Free Shear Flows," *The Global Geometry of Turbulence: Impact of Nonlinear Dynamics*, edited by J. Jimenez, Plenum, New York, 1991, pp. 3–11.

[32]Stine, H. A., and Winovich, W., "Light Diffusion Through High-Speed Turbulent Boundary Layers," NACA Research Memorandum A56B21, May 1956.

[33]Carslaw, H. S., and Jaeger, J. C., *Conduction of Heat in Solids*, Clarendon, Oxford, 1959, pp. 233–237.

[34]Hill, J. M., and Dewynne, J. N., *Heat Conduction*, Blackwell Scientific, Oxford, 1987, pp. 114–126, 143, 144.

J. P. Gore
Associate Editor